A Coral Diagenesis and Physiology Framework for Improving Coral $\delta^{18}O$ Paleoclimate Reconstructions

Luis G. Rodriguez[1], Alyssa R. Atwood[1], Kim M. Cobb[2], Hussein R. Sayani[1,3], and Pamela R. Grothe[4]

[1]Florida State University, Tallahassee, Florida, USA

[2]Brown University, Providence, Rhode Island, USA

[3]Langan Engineering and Environmental Inc, Parsippany, New Jersey, USA

[4]University of Mary Washington, Fredericksburg, Virginia, USA

Corresponding author: Luis G. Rodriguez (lgr19@fsu.edu)

Key Points:

- **A new framework utilizes diagenesis and physiology metrics to reduce uncertainty in mean coral d18O reconstructions**
- **The variance of a Holocene coral d18O record from Kiritimati is reduced by 46% and the uncertainty of the trend is reduced by 26%**
- **This framework has the potential to improve other paleoclimate reconstructions based on ensembles of mean coral d18O records**

Abstract

Reef-building corals provide seasonally resolved records of past climate variability from the ocean via variations in their oxygen isotope composition ($\delta^{18}O$). However, a variety of non-climatic factors can influence coral $\delta^{18}O$ including processes associated with coral biomineralization and post-depositional alteration of the coral skeleton, which add uncertainty to coral based paleoclimate reconstructions. These uncertainties are especially large in mean climate reconstructions developed from coral $\delta^{18}O$ values due to the large variability that exists in mean skeletal $\delta^{18}O$ signatures. We present a novel framework to minimize this uncertainty in mean coral $\delta^{18}O$ records based on a regression model that uses four commonly measured properties in coral skeletons and associated coral $\delta^{18}O$ records. We test the ability of the model to reduce noise in a Holocene climate reconstruction comprised of 37 coral $\delta^{18}O$ records from Kiritimati in the equatorial Pacific. Up to 43% of the variance in the detrended Holocene dataset is accounted for by a combination of four predictors: (1) mm-scale variability in a coral $\delta^{18}O$ record, (2) the physical extent of diagenetic alteration, (3) coral extension rate, and (4) the mean coral $\delta^{13}C$ value. Once these non-climatic artifacts are removed from the reconstruction, the weighted variance of the Holocene dataset is reduced by 46% and the uncertainty in the trend of coral $\delta^{18}O$ over time is reduced by 26%. These results have

important implications for the climate interpretation of this Holocene data set. This framework has the potential to improve other paleoclimate records based on ensembles of coral $\delta^{18}O$ records.

1 Introduction

Oxygen isotope ($\delta^{18}O$) records from massive reef-building corals are powerful tools for studying past climate variability in the tropical and subtropical oceans, extending as far back as the Pliocene (Watanabe et al., 2011). Coral $\delta^{18}O$ records form the cornerstone of ocean temperature reconstructions spanning several hundred years prior to the 19th-21st century, due to their relative abundance during this period and their monthly to annual resolution, which allows them to be robustly calibrated against instrumental data. Proxy system models for coral $\delta^{18}O$ further enhance their ability to be quantitatively compared to observational data and climate model output (Evans et al., 2000; Thompson et al., 2011; Dee et al., 2015). For this reason, coral $\delta^{18}O$ records are prevalent in most state-of-the-art paleoclimate reconstruction data sets, including those that merge multi-proxy datasets with paleo-data assimilation techniques (e.g., Konecky et al., 2020; Tardif et al., 2019; Tierney et al., 2015).

The oxygen isotopic composition of coral aragonite is a function of both the local sea surface temperature (SST) and the $\delta^{18}O$ of the surrounding seawater, which strongly covaries with sea surface salinity (SSS) (e.g., Epstein et al., 1953; Thompson et al., 2011; Thompson, 2022). As such, coral $\delta^{18}O$ is routinely used as a proxy for SST and/or SSS. However, while these records can provide powerful constraints on past SST and SSS variations, they can also be affected by a myriad of non-climatic processes. This includes coral 'vital effects,' which are associated with a variety of biomineralization processes that occur during coral calcification related to a combination of metabolic and kinetic processes (e.g., Felis et al., 2003;

McConnaughey, 1989), as well as post-depositional (diagenetic) alteration of the coral skeleton (e.g., McGregor & Gagan, 2003; Sherman et al., 1999).

Vital effects can lead to large offsets in mean coral $\delta^{18}O$ values in temporally overlapping colonies from the same reef (known as "intercolony offsets") (e.g., Allison et al., 1996; Cobb et al., 2003; Dassié et al., 2014; T. Felis et al., 2003; Stephans et al., 2004) and among differing growth transects within the same colony (De Villiers et al., 1995). These offsets in mean coral $\delta^{18}O$ values are a major source of uncertainty in coral-based paleoclimate reconstructions based on ensembles of coral records. Offsets in *Porites* spp. colonies can be as large as 0.4‰ (Cobb et al., 2003; Dassié et al., 2014; Linsley et al., 1999; Stephans et al., 2004), equivalent to a ~ 2°C offset in SST, using a $\delta^{18}O$/SST regression coefficient of -0.22‰/°C based on the empirical study of Lough (2004). One strategy for overcoming this uncertainty is to construct a composite record created by averaging multiple overlapping coral records across a given region (e.g., Dassié et al., 2014; Sayani et al., 2019); however, this approach is typically not feasible outside of the modern coral record, as sub-fossil corals (aka "fossil" corals) are sparse in space and time, and radiometric dating techniques add non-trivial age uncertainty.

The mechanisms for stable isotope vital effects remain an active area of research, but they have widely been attributed to growth rate dependent kinetic isotope fractionation during coral biomineralization, wherein rapid skeletal accretion imparts greater kinetic effects (T. McConnaughey, 1989b, 1989a; T. A. McConnaughey et al., 1997). It is well known that coral aragonite does not precipitate in equilibrium with the isotopic composition of seawater and is typically depleted in both $\delta^{13}C$ and $\delta^{18}O$ relative to seawater (e.g., Weber & Woodhead, 1972). The kinetic isotope effect is due to the light isotopologues diffusing faster than their heavy counterparts and reacting with other substances faster, and in biogenic carbonates it has been

linked to the CO_2 hydration and hydroxylation step during calcification, wherein when calcification occurs faster than the relatively slow hydration step can obtain isotopic equilibrium, the kinetic fractionation effect is preserved in the skeleton (McConnaughey, 1989a, 1989b). Biologically mediated speciation of the dissolved inorganic carbon pool in the calcifying fluid has also been proposed as a mechanism linking isotope fractionation to coral calcification rates (Adkins et al., 2003; Chen et al., 2018). Consistent with these mechanisms, an inverse relationship between coral $\delta^{18}O$ and skeletal growth rate, extension rate, and/or calcification rate has been found in a variety of studies, particularly in slow-growing corals (Allison et al., 1996; Cohen & Hart, 1997; Land et al., 1975; T. McConnaughey, 1989a; Diane M. Thompson, 2022; de Villiers et al., 1994; De Villiers et al., 1995). Several researchers have attempted to correct for growth-rate-related artifacts in coral-based paleoclimate reconstructions, (e.g., Felis et al., 2003; Westphal, 2015), while some studies find no significant relationship between growth rate and coral intercolony offsets (e.g. Sayani et al., 2019).

Vital effects also impact coral $\delta^{13}C$ values through metabolic and kinetic isotope effects (Schoepf et al., 2014) with kinetic isotope effects producing a strong correlation between $\delta^{18}O$ and $\delta^{13}C$ (Adkins et al., 2003; T. McConnaughey, 1989b). The direction of kinetic isotope disequilibrium is such that ^{12}C and ^{16}O are preferentially incorporated into the coral aragonite, yielding more negative $\delta^{13}C$ and $\delta^{18}O$ values than equilibrium values. Rapidly secreted biogenic carbonates, including corals with high calcification rates, can contain large kinetic isotope effects, as indicated by more negative $\delta^{18}O$ and $\delta^{13}C$ values and strong covariation between these values. Coral $\delta^{13}C$ is also affected by a myriad of other biologically mediated processes, including metabolic processes such as photosynthesis, respiration, and heterotrophy (Grottoli & Wellington, 1999; T. McConnaughey, 1989a; Swart, 1983). In rare cases, coral spawning events

are associated with significant but short-lived spikes towards higher $\delta^{18}O$ and $\delta^{13}C$ values in coral skeletons (e.g., Evans et al., 1999). This may be due to metabolic processes related to coral gamete production prior to spawning (e.g., Gagan et al., 1994) but as such signals are relatively uncommon, their precise origins remain unclear. Because some of these vital effects impact both coral $\delta^{13}C$ and $\delta^{18}O$ values, it may be possible to use coral $\delta^{18}C$ values to account for and remove or reduce the signature of vital effects from mean coral $\delta^{18}O$ records.

Diagenesis is another important source of uncertainty in coral $\delta^{18}O$ reconstructions. Coral skeletal diagenesis is a pervasive feature of most subfossil corals, as well as some modern corals, and can introduce large artifacts in coral $\delta^{18}O$-based climate reconstructions. In submarine environments, diagenesis typically takes the form of secondary aragonite cements, which precipitate inside the coral skeletal pore spaces from seawater (Cole et al., 1993; Gagan et al., 1998; Ren et al., 2002; Sayani et al., 2011; Weber & Woodhead, 1972). In subaerially exposed corals, dissolution of the primary skeletal aragonite can occur from exposure to meteoric and ground waters and is often followed by reprecipitation of secondary calcite. These processes can significantly alter the measured $\delta^{18}O$ value of the coral as abiogenic calcite and secondary aragonite precipitates have $\delta^{18}O$ values that differ appreciably from that of the original coral skeleton. Generally, submarine aragonite precipitates are characterized by more enriched $\delta^{18}O$ values, while subaerial diagenesis results in highly depleted $\delta^{18}O$ values linked to incorporation of isotopically light rainwater $\delta^{18}O$ in the recrystallized calcite (e.g., Sayani et al., 2011). Such diagenetic alteration can be present in both modern and fossil corals and lead to large errors in $\delta^{18}O$-derived SST reconstructions. For example, the presence of ~10% secondary aragonites by mass in modern corals from Palmyra and Fanning Island was found to yield biases in mm-scale $\delta^{18}O$ values of ~0.4‰, equivalent to ~ -2 ^{o}C (Sayani et al., 2011). Although it's standard practice

in paleoclimate studies to screen corals for diagenetic alteration using a variety of techniques such as X-ray imaging, X-Ray Powder Diffraction (XRD), Scanning Electron Microscope (SEM) imaging, and/or thin sections, these methods may not capture the entire sampling transect and/or capture microscale diagenesis features.

In this study, we develop and test a standardized method of separating the effects of diagenesis and coral vital effects from climate signals in mean coral $\delta^{18}O$ records using a small set of routinely measured metrics in an extensive suite of published coral $\delta^{18}O$ records spanning the last 6,400 years from Kiritimati in the central equatorial Pacific Ocean. Given the prevalence of coral $\delta^{18}O$ records in global and regional paleoclimate reconstructions (e.g., Cobb et al., 2003; McGregor et al., 2015; Reed et al., 2022; Jessica E. Tierney et al., 2015) and in recent paleoclimate data assimilation efforts (e.g. Steiger et al., 2018; Tardif et al., 2019), reducing the uncertainty in coral $\delta^{18}O$ records holds great value. Furthermore, the paucity of data from the central tropical Pacific in global temperature reconstructions of the Holocene (e.g., Marcott et al., 2013; Osman et al., 2021), coupled with the global footprint of tropical Pacific climate variations, warrant improving climate records from this region. To separate the climate and non-climate signals in the mean coral $\delta^{18}O$ record, we develop a series of simple screening metrics and incorporate them into a multivariate linear regression model for mean coral $\delta^{18}O$. Our goal is to quantify the effects of diagenesis and coral physiology on mean coral $\delta^{18}O$ and subsequently remove these effects from the Kiritimati coral $\delta^{18}O$ reconstruction. Because the predictor variables used in the regression model are routinely measured in coral paleoclimate studies, this method can be readily and broadly applied to other data sets to improve the climate constraints derived from ensembles of mean coral $\delta^{18}O$ records.

2 Methods

2.1 Data Sources

We employ an extensive collection of published coral $\delta^{18}O$ and $\delta^{13}C$ records from Kiritimati (2^{o} N, 157^{o} W) in the central equatorial Pacific Ocean in this study (Cobb et al., 2013; Evans et al., 1999; Grothe et al., 2020; Hitt et al., 2022). The records are divided into two categories based on age. The first category consists of modern and young fossil corals with ages between 1891 to 2003 CE (-53 to 59 yr BP), which are compiled in the "modern/20^{th} century" group (n = 10). The second category consists of older fossil corals with ages between 987 to 6400 yr BP, which are compiled in the "older fossil" group (n = 27). The modern coral records were collected from live coral colonies, while the fossil coral records were collected from coral heads that were washed ashore by intense wave activity (e.g., Cobb et al., 2003). Four criteria must be met for a given coral $\delta^{18}O$ record to be included in the dataset. The record must have: (1) a length greater than 60 mm, (2) mm-scale resolution coral $\delta^{18}O$ and $\delta^{13}C$ data, (3) at least two Scanning Electron Microscope (SEM) images with sufficient resolution to identify secondary aragonite precipitates in each coral, and (4) an estimate of the mean linear extension rate of the coral. After applying these criteria, the dataset comprises 37 coral $\delta^{18}O$ records spanning the last 6,400 years (Figure 1; Supplementary Table 1).

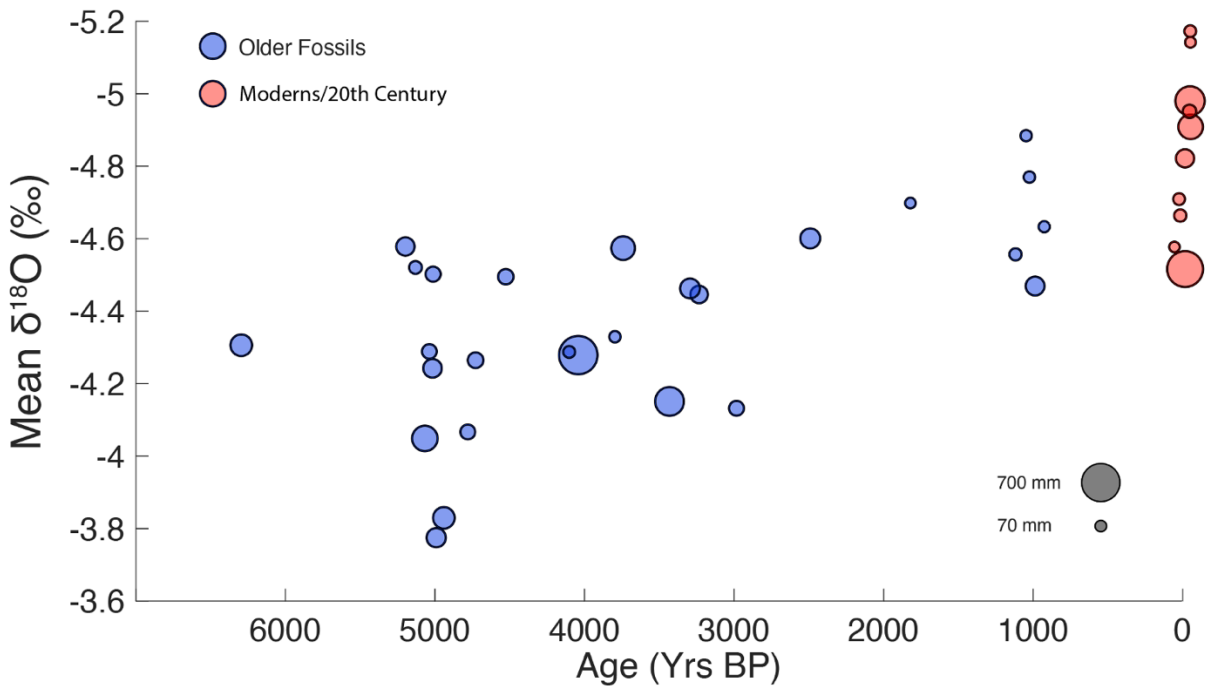

Figure 1. Mean coral $\delta^{18}O$ from Kiritimati spanning the last 6,400 years. The red symbols indicate the modern and 20th century records and the blue symbols indicate the older fossil records. The size of the symbols scales with the length of the coral records (in mm).

2.2 Predictor Variables of Mean Coral $\delta^{18}O$

We quantify the impact of diagenetic alteration and vital effects on mean coral $\delta^{18}O$ using a partial least square regression model trained on the set of predictors described below.

2.2.1 Scanning Electron Microscope estimates of diagenesis

The SEM image rating is described in detail in the supplementary methodology. Briefly, it assesses three aspects of diagenesis in SEM images to produce a numerical score for each coral record: (1) the fractional surface area of the SEM image covered with secondary aragonite (ASA), (2) the length of the secondary aragonite needles (LSA), and (3) the fractional surface area of the SEM image impacted by dissolution (DIS). Examples of these ratings are provided in Figure 2. To estimate the percentages of ASA and DIS in the SEM images, standard percent estimation guides commonly used in petrographic analysis are used to score the records from 5

(least altered) to 1 (most altered). The three individual SEM scores (ASA, LSA, DIS) are averaged to produce a combined SEM score, referred to as the combined SEM Diagenesis Score (COM). Calcite recrystallization is another important aspect of diagenesis to consider, however, in the coral records studied here, no evidence of calcite was found. This is likely because these published records have been screened for diagenesis prior to analysis using SEM and X-ray imaging and X-Ray Powder Diffraction (XRD).

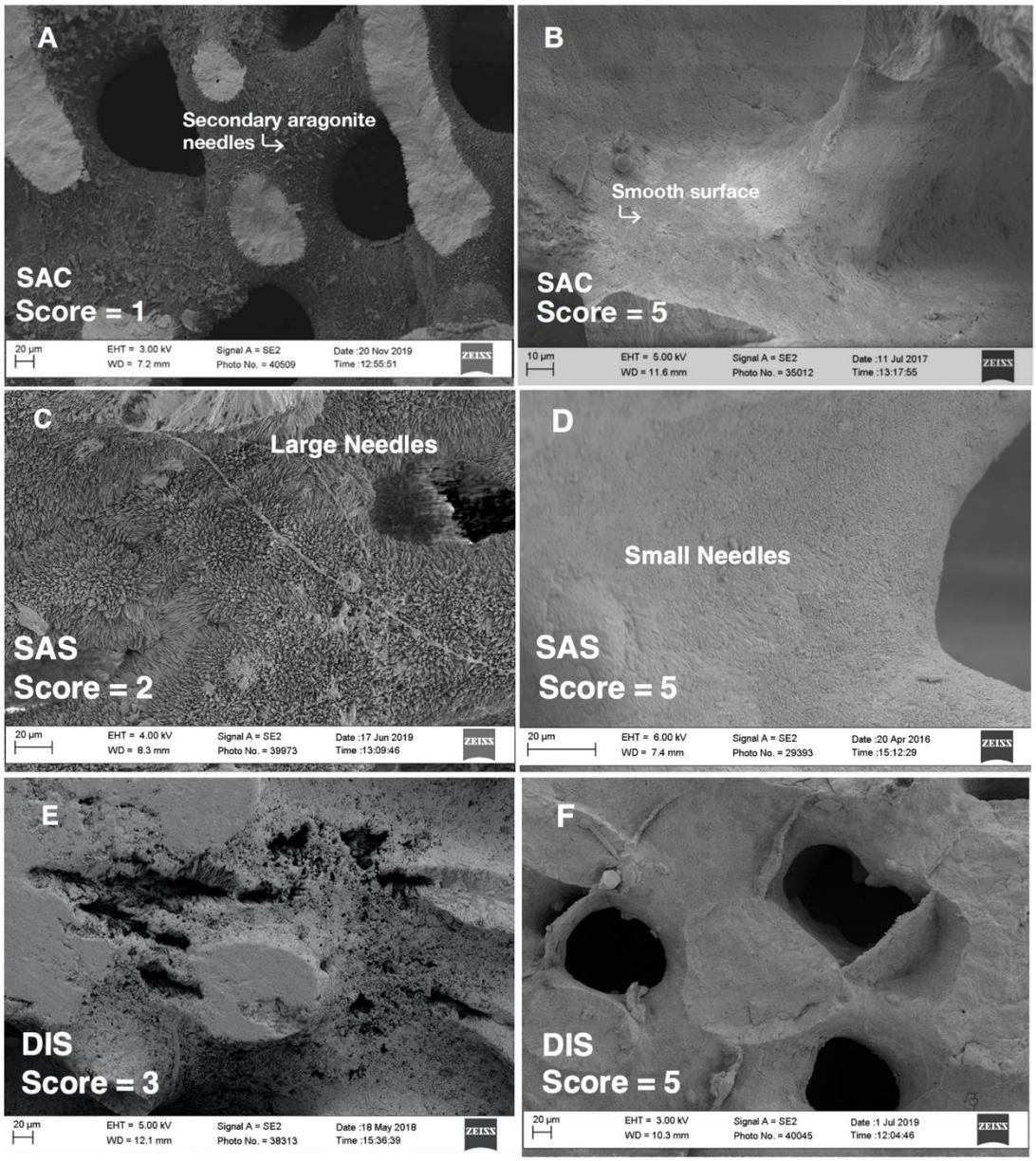

Figure 2. Examples of the SEM image rating categories. (A,B) Endmember examples of the ASA score (i.e. the surface area of the coral covered by secondary aragonite): (A) a coral with pervasive secondary aragonite growth versus (B) a pristine coral skeleton. (C,D) Examples of the LSA score (i.e. the length of the secondary aragonite needles): (C) a coral with large secondary aragonite needles versus (D) small secondary aragonite needles. (E,F) Examples of the dissolution score (DIS): (E) a coral impacted by dissolution versus (F) an intact skeleton.

177

178 2.2.2 Point to Point $\delta^{18}O$ Variability

179 Millimeter scale variability in the coral $\delta^{18}O$ records is impacted by widespread
180 diagenesis (which can evade detection in highly-localized SEM images) and coral spawning
181 events. In order to quantify mm-scale $\delta^{18}O$ variations, we apply a smoothing spline ($f = 0.07$) to
182 each coral record, which captures coral $\delta^{18}O$ variability on seasonal and longer timescales
183 (Figure 3 A,C,E). We then subtract the spline fit from the original $\delta^{18}O$ timeseries to isolate the
184 high-frequency noise in the $\delta^{18}O$ record. The 99th percentile of the absolute value of these offsets
185 define the mm-scale variability metric - hereafter referred to as the 'point-to-point variability'
186 (PTPV; Figure 3 B, D, F). The 99th percentile was chosen for this metric as it allows us to isolate
187 the largest class of deviations in the coral $\delta^{18}O$ records, which are closely associated with
188 diagenesis (Sayani et al., 2011) and coral spawning events (Evans et al., 1999).

189

190

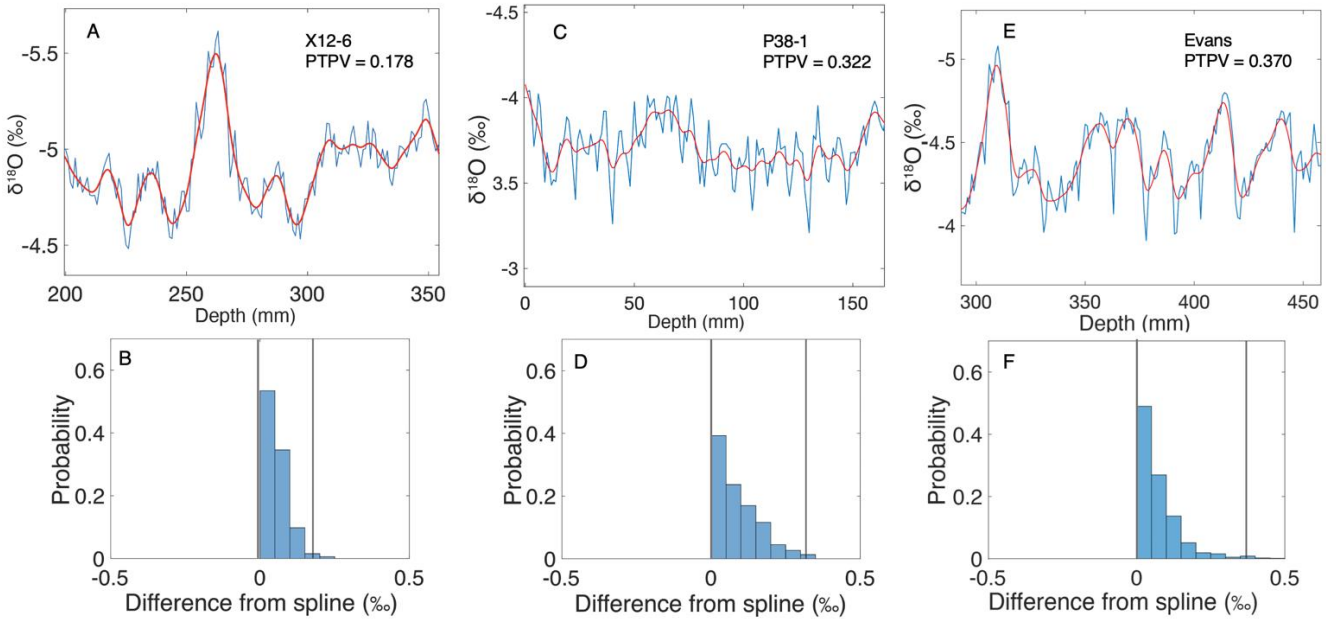

Figure 3. Examples of coral with low and high PTPV due to suspected diagenesis and coral spawning events. (A,C,E) The time series of the raw coral $\delta^{18}O$ record is shown in blue and the red curve is the spline fit to the data. (B,D,F) the probability distribution of the residuals (difference between the raw values and the spline fit). The rightmost black line represents the 99th percentile of the distribution (i.e. the PTPV value).

2.2.3 Mean Extension Rate

The mean extension rate of each coral record is calculated by dividing the length of the sampling transect (in millimeters) by the length of the coral record (in years), based on the chronology reported in the original publication of the dataset.

2.2.4 Mean $\delta^{13}C$ values

The mean $\delta^{13}C$ value for each coral record is calculated by averaging over the mm-scale $\delta^{13}C$ data (measured in tandem with the $\delta^{18}O$ data). Because the Suess effect drives a trend toward more depleted coral $\delta^{13}C$ values over the 20th century due to the input of anthropogenic CO_2 into the atmosphere and a corresponding decrease in $\delta^{13}C$ of dissolved inorganic carbon in the upper ocean (e.g. Dassié et al., 2014; Swart et al., 2010), we apply correction to the mean

coral $\delta^{13}C$ values for the 10 coral records in the modern and 20th century group using the linear trends presented in Dassié et al. (2014) and in Swart et al. (2010) based on a suite of tropical Pacific corals. Two sets of corrections are applied depending on the mean age of the corals, to account for the acceleration of the Suess effect over time. Corals with mean ages between 1966-2003 CE (-53 to -16 BP) are corrected using a slope of $-0.010‰yr^{-1}$ (which is the average of $-0.014‰yr^{-1}$ reported in Dassié et al. (2014) and -0.0066 ‰ yr^{-1} reported in Swart et al., 2010 for the period 1960-1990). Corals with mean ages between 1895-1959 CE (-17 BP to 55 BP) are corrected using a lower slope of $-0.005‰yr^{-1}$ (which is the average of $-0.0062‰yr^{-1}$ reported in Dassie et al. (2014) for the period 1900–1990 and -0.0037 ‰ yr^{-1} reported in Swart et al., 2010 for the period 1800-2000). The Suess effect corrections are subtracted from the original mean coral $\delta^{13}C$ values. The correction applied to the 10 modern and 20th century corals ranges from 0.00‰ for the oldest record (1895 CE) to -0.95‰ for the youngest record (2003 CE), with a mean correction of -0.49‰. This correction effectively eliminates the temporal slope in mean coral $\delta^{13}C$ over the 20th century (reducing the slope from -0.98‰ per century to -0.03‰ per century for the modern and 20th century records).

2.3 Partial Least Squares Regression Model

2.3.1 Model configuration

We construct a predictive model of mean coral $\delta^{18}O$ using the Partial Least Square Regression (PLSR) function **plsregress** in MATLAB, which uses the SIMPLS (Sequential Projection Algorithm for PLS) algorithm (de Jong, 1993; Wold et al., 2001). The SIMPLS algorithm in plsregress calculates M orthogonal linear combinations of the predictor variables (called “PLS components”) using an iterative method that maximizes the covariance between the response variable (here mean coral $\delta^{18}O$) and the predictor variables. It uses the method of least

squares to fit a linear regression model using a selected number of PLS components as predictors. Both the predictor and response variables are standardized prior to inclusion in the model. We use k-fold cross-validation with 1000 Monte Carlo repetitions to find the optimal number of PLS components to retain and evaluate the performance of the model. This cross-validation process randomly divides the set of observations into k=5 groups; the first group is treated as a validation dataset and the regression is trained on the remaining groups (e.g., de Jong, 1993; Wold et al., 2001). The mean square error (MSE) is then calculated between the observed mean coral $\delta^{18}O$ and model-predicted mean coral $\delta^{18}O$ from the validation dataset. The number of components that minimizes the MSE is adopted for the final model.

We make one assumption when using this regression model: homoscedasticity (i.e., the spread of the residuals vs. predicted values does not show an obvious trend or pattern) (Johnson & Wichern, 2002; Wilks, 2019; Wold et al., 2001). A primary advantage of PLS regression is that it is well-suited to data sets where there may be multicollinearity in the predictor values, such as the data set employed here (e.g., Michel et al., 2020; Wold et al., 2001; Xing et al., 2016).

We initially make one additional assumption specific to our dataset: the Holocene trend in mean coral $\delta^{18}O$ is a true climate signal unassociated with diagenesis or coral vital effects. Based on this assumption, the mean coral $\delta^{18}O$ data set is detrended before applying the PLS regression model. This detrending step removes the long-term trend in the Holocene dataset and leaves the coral $\delta^{18}O$ variability that exists on shorter (decadal to centennial) timescales. Due to the larger slope in the modern and 20th century records over the post-industrial era than that in the older fossil records over the Holocene, the detrending procedure is applied separately to the two age groups (the modern/20th century records and the older fossil records). Prior to their

introduction into the regression model, the predictor variables and detrended response variable are combined across the two age groups and then standardized by conversion to Z-scores (zero mean and standard deviation of unity) to provide consistent scaling between variables (Supplementary Table 1). The predicted value of mean coral $\delta^{18}O$ from the regression model is taken to be the component of the $\delta^{18}O$ value that is attributable to diagenesis and coral vital effects. These predicted values are therefore subtracted from the original mean $\delta^{18}O$ Z-scores to produce the 'corrected' mean $\delta^{18}O$ Z-scores. The corrected $\delta^{18}O$ Z-scores are then converted into raw $\delta^{18}O$ values (in units of per mille) by multiplying them by the standard deviation and then adding the mean of the original data. Lastly, the trend is added back to the data set to produce the final corrected reconstruction of mean coral $\delta^{18}O$. To test the sensitivity of the results to this detrending step, the procedure is repeated without detrending the data and the results of the detrended and non-detrended version of the model are compared.

2.3.2 Model Calibration

To calibrate the mean $\delta^{18}O$ corrections obtained from the PLS model, a uniform offset of +0.16‰ is applied to the corrections obtained such that the average correction of two pristine modern corals (X12-3 and X12-6) is zero (Figure S1) (Grothe et al., 2020). These corals were chosen as the calibration benchmark for the model because these corals show the least amount of diagenetic alteration in the compilation and are known to track local temperature variations in Kiritimati closely. This calibration offset is relatively small compared to the range of corrections applied across the coral dataset (-0.47‰ to +0.05‰; Table S1).

3 Results and Discussion

3.1 Mean coral $\delta^{18}O$ trends and variability

Prior to applying our correction methodology, the Kiritimati mean coral $\delta^{18}O$ record displayed a prominent secular negative (depletion) trend from 6,400 yr BP to the present (Figure 1). This trend implies a trend toward warmer and/or wetter conditions from the mid-Holocene to present. Around this long-term trend, there are pronounced short-term (decadal to centennial scale) variations in mean coral $\delta^{18}O$ that are of comparable magnitude to the trend itself. Specifically, the long-term trend in mean coral $\delta^{18}O$ is 0.62‰ from the mid-Holocene to present and the trend over the 20th century is 0.46‰/century, while the range in mean coral $\delta^{18}O$ in 50-yr windows in the dataset reaches up to 0.51‰ (maximizing from 4985-5035 yr BP). Given the capacity of diagenesis and coral vital effects to dramatically alter coral $\delta^{18}O$, it is feasible that a significant portion of this variability in mean coral $\delta^{18}O$ is the result of non-climate-related processes. To minimize their impact on the mean coral $\delta^{18}O$ record, we invoke a partial least square regression model with a small set of predictors related to diagenesis and coral vital effects to quantify their effects and subsequently remove these effects from the reconstruction.

3.2 Optimizing the PLS regression model

Six predictor variables (ASA, LSA, COM, PTPV, C13, and Extension Rate) were evaluated as predictors of mean coral $\delta^{18}O$ using the PLS model. The optimal predictors were found by testing the model with different combinations of predictors and calculating the mean square error (MSE) between the resulting predicted and observed mean coral $\delta^{18}O$ values, using five-fold cross validation. Dissolution (DIS) was not included in these tests as only a few coral records showed minimal dissolution features, making it unsuitable as a predictor. The combination that yielded the lowest MSE was ASA, PTPV, C13, and Extension Rate and thus

these were chosen as the final predictors for the model (Figure S2 A, B). In this configuration, the residuals of the response variable (i.e. the difference between the predicted and observed mean coral $\delta^{18}O$ values) show no apparent trend or pattern, indicating that the model's assumptions are fulfilled in our application (Figure S2C). As indicated by the loadings of the four predictor variables (Figure S3A), PTPV and C13 provide the largest contribution to predicted mean coral $\delta^{18}O$, while Extension Rate and ASA (the fractional area of secondary aragonite) provide smaller contributions. The relative importance of the predictors to the final correction is shown in Figure S4. The clear dominance of the PTPV metric may be because of its ability to capture both diagenesis and coral spawning events in the coral records (Figure 3C-F).

The predicted mean coral $\delta^{18}O$ calculated from the PLS model is significantly correlated with the observed mean coral $\delta^{18}O$ ($R^2 = 0.43$, $p < 0.001$) (Figure 4), indicating that the four chosen metrics of diagenesis and coral vital effects (related to PTPV, mean $\delta^{13}C$, extension rate, and diagenetic condition) together explain 43% of the variance in mean coral $\delta^{18}O$ values across coral records in the Holocene dataset. The remainder of the mean coral $\delta^{18}O$ variability is attributed to climate variations.

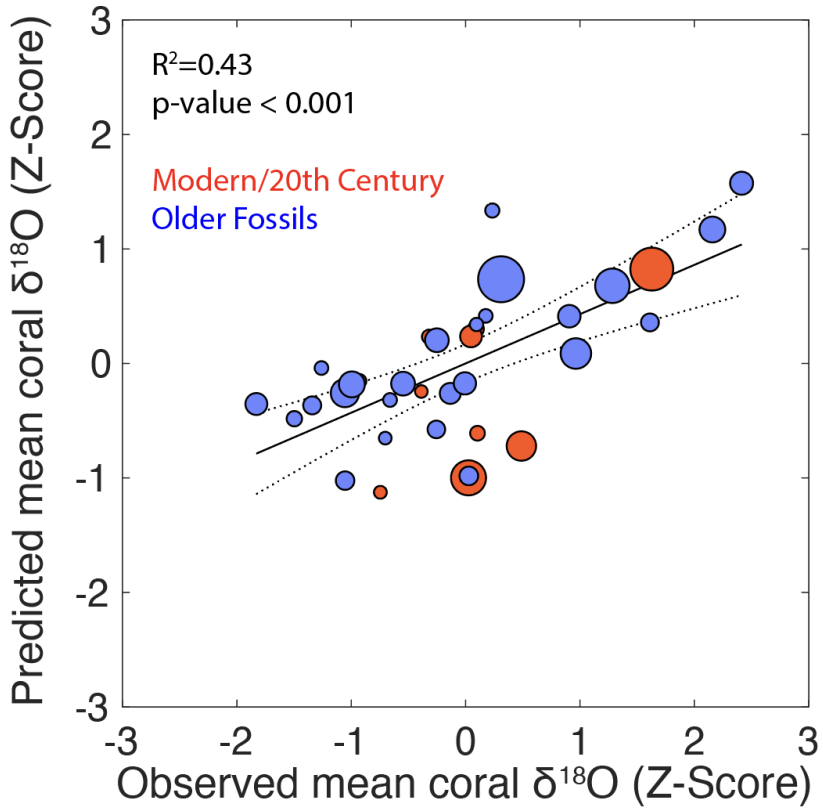

Figure 4. Predicted mean coral $\delta^{18}O$ from the PLS regression model versus observed mean coral $\delta^{18}O$ (as Z-scores), plotted with the best fit linear regression line and the 95% confidence intervals around the slope.

3.3 Mean coral $\delta^{18}O$ corrections

The regression model predicts the mean coral $\delta^{18}O$ value expected based on each coral record's PTPV, mean $\delta^{13}C$, extension rate, and diagenetic condition. This predicted $\delta^{18}O$ value is taken to be the component of the mean coral $\delta^{18}O$ that is attributable to diagenesis and coral vital effects. The predicted value is therefore subtracted from the original $\delta^{18}O$ value to produce a 'corrected' $\delta^{18}O$ value of each coral record. The correction applied to each coral ranges from -0.47‰ to +0.05‰ (Table S1; Figure S1A) which if interpreted solely in terms of temperature using a coral $\delta^{18}O$/temperature scaling of -0.22‰/°C (Lough, 2004; Thompson et al., 2011), provides a temperature correction of -0.45°C to +2.10°C. These corrections are within the range

of reported variation associated with diagenesis and intercolony offsets reported in prior studies (Cobb et al., 2003; Dassié et al., 2014; Felis & Patzold, 2004; Linsley et al., 1999; Stephans et al., 2004, McGregor & Gagan, 2003; Sayani et al., 2011). The corrections are largely negative and therefore shift the data towards more depleted $\delta^{18}O$ values (Figure 5; Figure S1A), consistent with an enrichment bias in the original $\delta^{18}O$ values driven by the presence of secondary aragonite precipitates (e.g., Sayani et al., 2011). In addition, the enrichment bias could be amplified by the presence of spawning events in some coral records, which are associated with highly enriched seasonal spikes in $\delta^{18}O$ (Figure 3E). As expressed in the loadings of the PLS model, the correction is primarily driven by PTPV and mean $\delta^{13}C$, and secondarily by the SEM rating (ASA) and Extension Rate (Figure S3A; Figure S4A).

The effect of the corrections on the Holocene data set is evaluated in two ways. We evaluate the change in weighted variance of the detrended mean coral $\delta^{18}O$ values over the Holocene, which is a measure of the coral-to-coral variability in the data set. The variance is weighted by the length of the coral records, since longer records provide a more robust estimate of mean climate. This weighting scheme is consistent with that performed in coral $\delta^{18}O$-based ENSO reconstructions over the Holocene (Grothe et al., 2019). We also evaluated the change in the 95% confidence interval of the trend in mean coral $\delta^{18}O$ over the Holocene, which is a measure of the uncertainty of the long-term temporal trend in the Holocene dataset.

When all the data are combined, the weighted variance of the detrended mean coral $\delta^{18}O$ in the Holocene data set is reduced by 46% and the confidence interval of the slope (of the re-trended data) is reduced by 26%, relative to the original set (Table 1; Figure 5). The same analysis is performed on the modern/20th century and older fossil groups separately. In the

dataset comprised of the 10 modern/20th century corals, the weighted variance is reduced by 51% and the confidence interval of the slope is decreased by 6% (Table 1; Figure S5). The large reduction in weighted variance in this group is primarily due to the large negative correction applied to the long (780 mm) record from Evans et al. (1999), which shifts that record close to the trend line (Figure S5). In the older fossils, the weighted variance is reduced by 54% and the confidence interval around the slope is reduced by 30%. Large negative corrections to several long coral records in the 3-5 ka interval with substantial evidence of mm-scale diagenesis as represented by their high PTPV values (e.g. P38-1, P38-2, p34, P43; Figure 3C; Figure. 5; Table S1) were largely responsible for the reduction in weighted variance and reduction in confidence interval in the older fossil group.

Table 1. Weighted variance, slope, and 95% confidence intervals in the original and corrected mean coral $\delta^{18}O$ data sets. The weighted variance is calculated from the detrended data to reflect centennial-scale variability.

Grouping	Detrended Weighted Variance (‰²)	Change in Weighted Variance	Slope (‰/millenia)	Change in slopes	Range of Confidence Interval (‰)	Change in the Confidence Interval range
Original $\delta^{18}O$ - All	0.04		0.117		0.06	
Corrected $\delta^{18}O$ - All	0.02	-46%	0.110	-6%	0.04	-26
Original $\delta^{18}O$ - Mod/20thCent	0.02		4.621		0.47	
Corrected $\delta^{18}O$ - Mod/20thCent	0.01	-51%	3.716	-20%	0.44	-6
Original $\delta^{18}O$ - Fossils	0.04		0.100		0.09	
Corrected $\delta^{18}O$ - Fossil	0.02	-54%	0.107	7%	0.06	-30

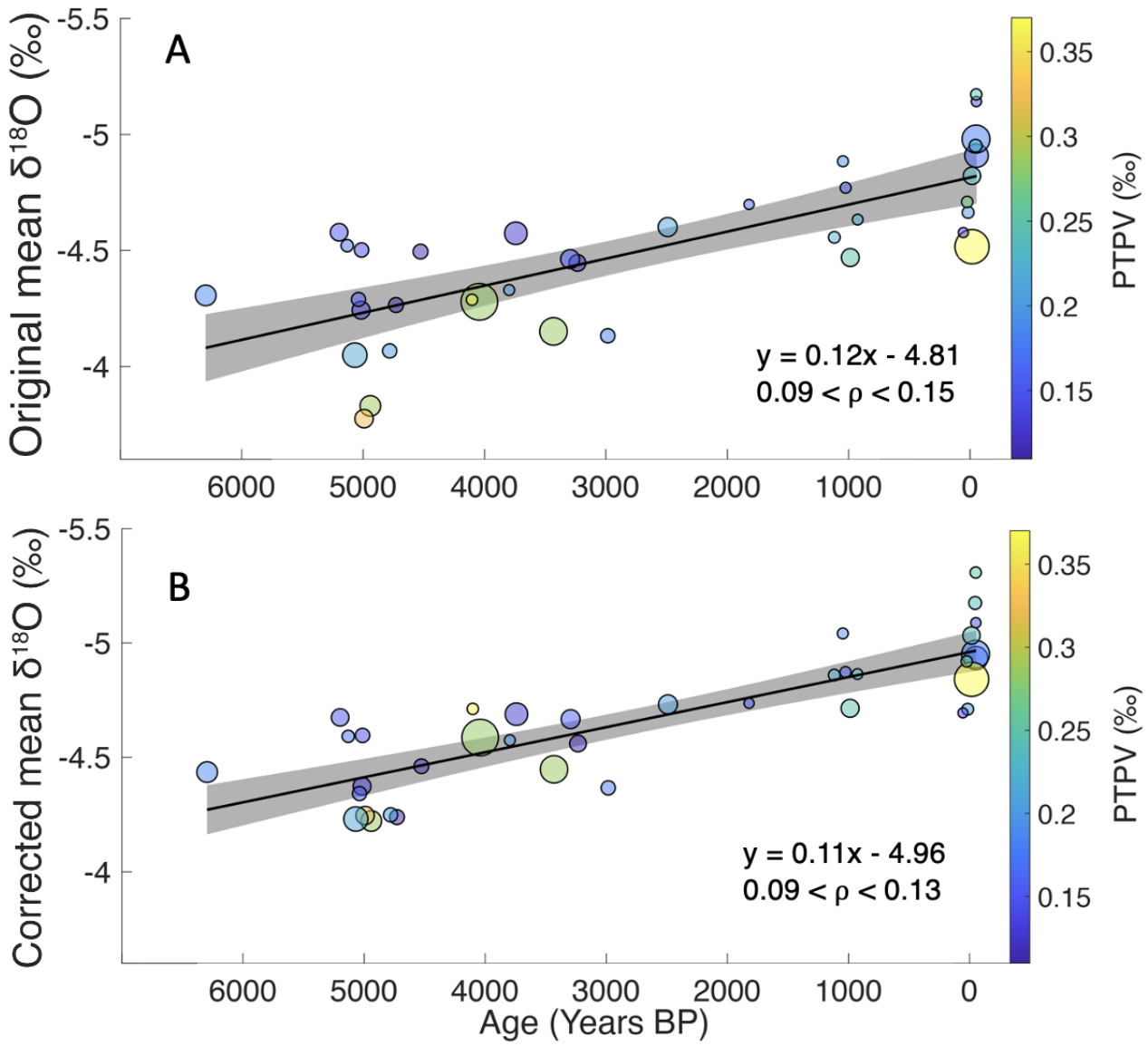

Figure 5. Mean coral $\delta^{18}O$ values in the original dataset (A) and the corrected dataset (B). The coral records are colored according to the magnitude of PTPV in each record. The size of the symbols corresponds to the length of the record (ranging from 70mm to 700mm), the line represents the linear trend, and the shading represents the 95% confidence interval around the slope. The equation of the trend line is provided, along with the values of the 95% confidence interval. X represents the age in thousands of years.

371 The fossil corals are further separated into three age groups (900-1200 BP, 2900-4200
372 BP, and 4500-5200 BP) to provide a more in-depth assessment of the reduction in inter-coral
373 variability at centennial timescales in the Holocene record. These groups (Fossil Groups 1, 2 and
374 3) were chosen based on periods of highest sample density. Fossil Groups 1, 2 and 3 show a
375 reduction of the weighted variance of -46%, -56%, and -66% respectively (Table S2; Figure S8).
376 These results demonstrate that the corrections produce a clear and relatively consistent reduction
377 in inter-coral variability at centennial timescales across the Holocene record, resulting in
378 improved isolation of the climate signal relative to the non-climatically driven noise associated
379 with diagenesis and coral vital effects.

380

381 3.4 Sensitivity of the correction to detrending

382 Our application of the model results assumes that the long-term trend in mean coral $\delta^{18}O$
383 of -0.12‰/millennia observed in Holocene dataset and the larger trend of -0.46‰/century in the
384 20^{th} Century/Modern dataset are driven by climate variations and not diagenesis and coral vital
385 effects (Figure 5 and S5). By detrending the dataset prior to training the model and then adding
386 the trend back in after the data have been corrected, the original trend in the data is largely
387 preserved (Fig. 5; Table 1). However, it is unknown the degree to which the trend in mean coral
388 $\delta^{18}O$ over time through the Holocene may be related to diagenesis and/or coral vital effects (e.g.
389 changes in coral growth rate).

390

391 To test the sensitivity of the results to this assumption, the regression model is retrained
392 and reapplied to the coral data without first detrending the data. In this "non-detrended" version

of the model, the model-predicted corrections produce a 38% reduction in the long-term trend in mean coral $\delta^{18}O$ (from 0.12‰/millennia to 0.07 ‰/millennia; Fig. S6) and a 53% reduction in the trend in mean coral $\delta^{18}O$ over the 20th century (from 0.46‰/century to 0.22‰/century; Figure S7).

These differences are a result of a pronounced correlation between the SEM diagenesis score (ASA) and coral age over the Holocene, indicating that older corals have more diagenetic alteration. When the trend in the mean coral $\delta^{18}O$ data is retained, the PLS regression model captures and attempts to correct for the relationship between ASA and mean coral $\delta^{18}O$, and because ASA is also strongly correlated to age, the model produces a large correction to older corals that tend to have more extensive secondary aragonite coverage. This can be seen in the predictor loadings, which are largest for the ASA metric in this version of the model. The loading for the $\delta^{13}C$ metric is also substantial, while the loadings for PTPV and extension rate are smaller (Figure S3B).

The magnitude of the corrections also increases dramatically in the non-detrended version of the model (Figure S1B), reaching values well above the range of expected deviations in $\delta^{18}O$ based on coral diagenesis and inter-colony variability (Figure S1B). These results call into question the validity of this model and suggest that the model configuration that includes the detrended step may be more justifiable.

However, it is ultimately unknown the degree to which the trend in mean coral $\delta^{18}O$ over time through the Holocene may be related to diagenesis and/or coral vital effects (e.g. through changes in coral growth rate over time). Thus, to account for this uncertainty, we report both sets of trends, using the detrended methodology as an upper bound on the mean climate

reconstruction and the non-detrended methodology as a lower bound. The upper bound assumes that the long-term Holocene trend in mean $\delta^{18}O$ is due entirely to climate changes, while the lower bound assumes that a substantial portion of this trend is due to a combination of diagenesis and coral vital effects. The upper bound on the trend is 0.11‰/millennia (or 0.50°C/millennia of warming when interpreted in terms of temperature using a scaling -0.22‰/°C (e.g., Lough, 2004; Thompson et al., 2011)). The lower bound of the trend is 0.07‰/millennia (or 0.32°C/millennia warming) over the Holocene.

Comparing these mean climate trends to previous tropical Pacific SST reconstructions over the Holocene demonstrates that the upper and lower bounds of our reconstruction imply significantly faster warming than that estimated by the multi-proxy SST reconstruction of Gill et al. (2016) (0.03-0.09°C/millennia in the Niño 3.4 region over the 6000-2000 yr BP overlapping timespan of the reconstructions). In that study, foraminifera and alkenone records from the eastern and western equatorial Pacific were combined using a reduced-dimension approach to reconstruct full-field SSTs in the tropical Pacific. This discrepancy may be due to the lack of proxy data from the central Pacific in the Gill et al. (2016) reconstruction, the different spatial scales captured by the different reconstruction techniques, and/or biases across different proxy types, including in our coral $\delta^{18}O$ records, which reflect a combination of both temperature and seawater $\delta^{18}O$ changes over the Holocene. For example, our assumption of a constant scaling coefficient between coral $\delta^{18}O$ and temperature of -0.22‰/°C may be an invalid assumption on these long (millennial) timescales.

To contextualize the 20th century climate trends in our reconstruction, we compare our results to the Kiritimati coral $\delta^{18}O$ reconstructions from Hitt et al. (2022), noting that many of the 20th century records in this analysis were taken from that study. Our upper and lower bounds of

438 0.32‰/century and 0.22‰/century (1.45°C/century and 0.9°C/century respectively) bracket the
439 reported trend of 0.33 ± 0.03‰ (2σ) (1.45 ± 0.28°C) over the 20th century in Hitt et al. (2022).
440 These inferred SST trends are much greater than the 0.01°C - 0.55°C per century SST trends
441 observed in a range of observational reanalysis data products for the central equatorial Pacific
442 over the 20th century (Hitt et al., 2022). This discrepancy has been attributed to significant
443 freshening of seawater in the central tropical Pacific over the late 20th century. Future studies that
444 pair coral $\delta^{18}O$ with Sr/Ca data would enable separation of the temperature and seawater $\delta^{18}O$
445 components of the coral $\delta^{18}O$ trends.

446 **4 Conclusions**

447 We have developed a simple and standardized framework to isolate and remove the
448 effects of diagenesis and coral vital effects in mean climate reconstructions based on coral $\delta^{18}O$.
449 This framework employs commonly used metrics of diagenesis that are routinely measured by
450 coral researchers in tandem with a multivariate linear regression model. Application of this
451 method to mean coral $\delta^{18}O$ records from Kiritimati spanning the Holocene yields significant
452 reduction in inter-coral variability in mean $\delta^{18}O$ driven by diagenesis and coral vital effects.
453 When the effects of these non-climatic artifacts are accounted for and removed from the
454 reconstruction, the centennial scale variance in mean coral $\delta^{18}O$ is reduced by 46% to 66%, the
455 weighted variance across the entire dataset is reduced by 46%, and the uncertainty in the long-
456 term Holocene trend is reduced by 26%.

457 Although the model leads to a dramatic improvement in the mean coral $\delta^{18}O$
458 paleoclimate reconstruction by reducing non-climate related variability driven by diagenesis and
459 coral vital effects, other uncertainties in the reconstruction remain that cannot be addressed by

our methodology- namely uncertainty in the contributions of temperature and seawater $\delta^{18}O$ variations to the coral $\delta^{18}O$ records. This emphasizes the need for more robust Holocene temperature reconstructions from this region (e.g. based on coral Sr/Ca or Sr-U measurements) to allow both temperature and seawater $\delta^{18}O$ variations to be reconstructed over the Holocene. However, the notable success of this method in reducing the noise in mean coral $\delta^{18}O$ reconstructions suggests that the method may also be applicable to other coral-based paleoclimate proxies, such as coral Sr/Ca records, which are even more heavily affected by diagenetic alteration than coral $\delta^{18}O$.

Acknowledgments

Support for this work was provided to Alyssa Atwood by the National Science Foundation under award OCE-1903640. We wish to thank Aaron Jones for aiding with SEM imaging and XRD sample preparation.

Open Research

The high-resolution coral $\delta^{18}O$ and $\delta^{13}C$ records from Kiritimati used in this study are compiled from Cobb et al. (2013), Evans et al. (1999), Grothe et al. (2020), Hitt et al. (2022), or obtained directly from the authors (see Supplementary Table 1). The analyses are performed using the Matlab script provided at: https://figshare.com/s/ca64106594f6d75342b3 using the data in Supplementary Table 1 provided here: https://figshare.com/s/adaeaaff689d8433257e.

References

Adkins, J., Boyle, E., Curry, W., & Lutringer, A. (2003). Stable isotopes in deep-sea corals and a new mechanism for "vital effects" Stable isotopes in deep-sea corals and a new mechanism for "vital effects" Stable Isotopes in Deep-Sea Corals and a New Mechanism for "Vital Effects." *Geochimica et Cosmochimica Acta*, *67*(6), 1129–1143. https://doi.org/10.1016/S0016-7037(02)01203-6ï

Allison, N., Tudhope, A., & Fallick, A. E. (1996). Factors influencing the stable carbon and oxygen isotopic composition of Porites lutea coral skeletons from Phuket, South Thailand. *Coral Reefs*, *15*(1), 43–57. Retrieved from https://www.research.ed.ac.uk/en/publications/factors-influencing-the-stable-carbon-and-oxygen-isotopic-composi

Cobb, K. M., Charles, C. D., Cheng, H., & Edwards, R. L. (2003). El Niño/Southern Oscillation and tropical Pacific climate during the last millennium. *Nature*, *424*(6946), 271–276. https://doi.org/10.1038/nature01779

Cobb, K. M., Westphal, N., Sayani, H. R., Watson, J. T., Di Lorenzo, E., Cheng, H., et al. (2013). Highly variable El Niño-Southern Oscillation throughout the Holocene. *Science*, *339*(6115), 67–70. https://doi.org/10.1126/science.1228246

Cohen, A. L., & Hart, S. R. (1997). The effect of colony topography on climate signals in coral skeleton. *Geochimica et Cosmochimica Acta*, *61*(18), 3905–3912. https://doi.org/10.1016/S0016-7037(97)00200-7

Dassié, E. P., Linsley, B. K., Corrège, T., Wu, H. C., Lemley, G. M., Howe, S., & Cabioch, G. (2014). A Fiji multi-coral δ 18 O composite approach to obtaining a more accurate reconstruction of the last two-centuries of the ocean-climate variability in the South Pacific Convergence Zone region. https://doi.org/10.1002/2013PA002591

Epstein, B. S., Buchsbacm, J., Lowenstam, H. A., & Ukey, H. C. (1953). Revised carbonate-water isotopic temperature scale, *64*, 1315–1326.

Evans, M. N., Fairbanks, R. G., & Rubenstone, J. L. (1999). The thermal oceanographic signal of El Niño reconstructed from a Kiritimati Island coral. *Journal of Geophysical Research: Oceans*, *104*(C6), 13409–13421. https://doi.org/10.1029/1999JC900001

Felis, T., Pätzold, J., & Loya, Y. (2003a). Mean oxygen-isotope signatures in Porites spp. corals: Inter-colony variability and correction for extension-rate effects. *Coral Reefs*, *22*(4), 328–336. https://doi.org/10.1007/S00338-003-0324-3/FIGURES/4

Felis, T., Pätzold, J., & Loya, Y. (2003b). Mean oxygen-isotope signatures in Porites spp. corals: Inter-colony variability and correction for extension-rate effects. *Coral Reefs*, *22*(4), 328–336. https://doi.org/10.1007/S00338-003-0324-3/METRICS

Felis, Thomas, & Patzold, J. (2004). Climate Reconstructions from Annually Banded Corals. *Global Environmental Change in the Ocean and on Land*, 205–227.

Gagan, M. K., Chivas, A. R., & Isdale, P. J. (1994). EPSL High-resolution isotopic records from corals using ocean temperature and mass-spawning chronometers. Earth and Planetary Science Letters (Vol. 121).

Grothe, P. R., Cobb, K. M., Liguori, G., Di Lorenzo, E., Capotondi, A., Lu, Y., et al. (2020). Enhanced El Niño–Southern Oscillation Variability in Recent Decades. *Geophysical Research Letters*, *47*(7). https://doi.org/10.1029/2019GL083906

Grottoli, A. G., & Wellington, G. M. (1999). Effect of light and zooplankton on skeletal 13 C values in *the eastern Pacific corals Pavona clavus* and *Pavona gigantea*. Coral Reefs (Vol. 18). Springer-Verlag.

Hitt, N. T., Sayani, H. R., Atwood, A. R., Grothe, P. R., Maupin, C., O'Connor, G. K., et al. (2022, January 16). Central Equatorial Pacific Warming and Freshening in the Twentieth Century: Insights From a Coral Ensemble Approach. *Geophysical Research Letters*. John Wiley and Sons Inc. https://doi.org/10.1029/2021GL094051

Johnson, R. A., & Wichern, D. W. (2002). *Applied Multivariate Statistical Analysis*. Prentice Hall. Retrieved from https://books.google.com/books?id=VlcZAQAAIAAJ

de Jong, S. (1993). SIMPLS: an alternative approach squares regression to partial least, *18*, 2–263.

Land, L. S., Lang, J. C., & Barnes, D. J. (1975). Extension rate: A primary control on the isotopic composition of West Indian (Jamaican) scleractinian reef coral skeletons. *Marine Biology*, *33*(3), 221–233. https://doi.org/10.1007/BF00390926/METRICS

Linsley, B. K., Messier, R. G., & Dunbar, R. B. (1999). Assessing between-colony oxygen isotope variability in the coral Porites lobata at Clipperton Atoll. *Coral Reefs*, *18*, 13–27.

Marcott, S. A., Shakun, J. D., Clark, P. U., & Mix, A. C. (2013). A Reconstruction of Regional. *Science (New York, N.Y.)*, *339*(6124), 1198–1201. https://doi.org/10.1126/science.1228026

McConnaughey, T. (1989a). 13C and 18O isotopic disequilibrium in biological carbonates: I. Patterns. *Geochimica et Cosmochimica Acta*, *53*(1), 151–162. https://doi.org/10.1016/0016-7037(89)90282-2

McConnaughey, T. (1989b). 13C and 18O isotopic disequilibrium in biological carbonates: II. In vitro simulation of kinetic isotope effects. *Geochimica et Cosmochimica Acta*, *53*(1), 163–171. https://doi.org/10.1016/0016-7037(89)90283-4

McConnaughey, T. A., Burdett, J., Whelan, J. F., & Paull, C. K. (1997). Carbon isotopes in biological carbonates: Respiration and photosynthesis. *Geochimica et Cosmochimica Acta*, *61*(3), 611–622. https://doi.org/10.1016/S0016-7037(96)00361-4

Mcgregor, H. V, & Gagan, M. K. (2003). Diagenesis and geochemistry of Porites corals from Papua New Guinea: Implications for paleoclimate reconstruction. https://doi.org/10.1016/S0016-7037(02)01050-5

McGregor, H. V., Evans, M. N., Goosse, H., Leduc, G., Martrat, B., Addison, J. A., et al. (2015). Robust global ocean cooling trend for the pre-industrial Common Era. *Nature Geoscience 2015 8:9*, *8*(9), 671–677. https://doi.org/10.1038/ngeo2510

Michel, S., Swingedouw, D., Chavent, M., Ortega, P., Mignot, J., & Khodri, M. (2020). Reconstructing climatic modes of variability from proxy records using ClimIndRec version 1.0. *Geoscientific Model Development*, *13*(2), 841–858. https://doi.org/10.5194/GMD-13-841-2020

Osman, M. B., Tierney, J. E., Zhu, J., Tardif, R., Hakim, G. J., King, J., & Poulsen, C. J. (2021). Globally resolved surface temperatures since the Last Glacial Maximum. *Nature 2021 599:7884*, *599*(7884), 239–244. https://doi.org/10.1038/s41586-021-03984-4

Reed, E. V., Thompson, D. M., & Anchukaitis, K. J. (2022). Coral-Based Sea Surface Salinity Reconstructions and the Role of Observational Uncertainties in Inferred Variability and Trends. *Paleoceanography and Paleoclimatology*, *37*(6), e2021PA004371. https://doi.org/10.1029/2021PA004371

Sayani, H. R., Cobb, K. M., Cohen, A. L., Elliott, W. C., Nurhati, I. S., Dunbar, R. B., et al. (2011). Effects of diagenesis on paleoclimate reconstructions from modern and young fossil corals. *Geochimica et Cosmochimica Acta*, *75*(21), 6361–6373. https://doi.org/10.1016/j.gca.2011.08.026

Sayani, H. R., Cobb, K. M., DeLong, K., Hitt, N. T., & Druffel, E. R. M. (2019). Intercolony δ18O and Sr/Ca variability among Porites spp. corals at Palmyra Atoll: Toward more robust coral-based estimates of climate. *Geochemistry, Geophysics, Geosystems*, *20*(11), 5270–5284. https://doi.org/10.1029/2019GC008420

Schoepf, V., Levas, S. J., Rodrigues, L. J., McBride, M. O., Aschaffenburg, M. D., Matsui, Y., et al. (2014). Kinetic and metabolic isotope effects in coral skeletal carbon isotopes: A re-evaluation using experimental coral bleaching as a case study. *Geochimica et Cosmochimica Acta*, *146*, 164–178. https://doi.org/10.1016/j.gca.2014.09.033

Sherman, C. E., Fletcher, C. H., & Rubin, K. H. (1999). Marine and meteoric diagenesis of Pleistocene carbonates from a nearshore submarine terrace, Oahu, Hawaii.

Steiger, N. J., Smerdon, J. E., Cook, E. R., & Cook, B. I. (2018). A reconstruction of global hydroclimate and dynamical variables over the Common Era. *Scientific Data 2018 5:1*, *5*(1), 1–15. https://doi.org/10.1038/sdata.2018.86

Stephans, C. L., Quinn, T. M., Taylor, F. W., & Corrège, T. (2004). Assessing the reproducibility of coral-based climate records. *Geophysical Research Letters*, *31*(18). https://doi.org/10.1029/2004GL020343

Swart, P. K. (1983). *Carbon and Oxygen Isotope Fractionation in Scleractinian Corals: a Review*.

Tardif, R., Hakim, G. J., Perkins, W. A., Horlick, K. A., Erb, M. P., Emile-Geay, J., et al. (2019). Last Millennium Reanalysis with an expanded proxy database and seasonal proxy modeling. *Climate of the Past*, *15*(4), 1251–1273. https://doi.org/10.5194/CP-15-1251-2019

Thompson, D M, Ault, T. R., Evans, M. N., Cole, J. E., & Emile-Geay, J. (2011). Comparison of observed and simulated tropical climate trends using a forward model of coral d 18 O. https://doi.org/10.1029/2011GL048224

Thompson, Diane M. (2022). Environmental records from coral skeletons: A decade of novel insights and innovation. *Wiley Interdisciplinary Reviews: Climate Change*, *13*(1), e745. https://doi.org/10.1002/WCC.745

Tierney, J. E., Abram, N. J., Anchukaitis, K. J., Evans, M. N., Giry, C., Kilbourne, K. H., et al. (2015). Tropical Corals 400 yrs reconstructed from coral archives. *Paleoceanography*, *30*(October), 226–252. https://doi.org/10.1002/2014PA002717.Received

de Villiers, S., Shen, G. T., & Nelson, B. K. (1994). The SrCa-temperature relationship in coralline aragonite: Influence of variability in (SrCa)seawater and skeletal growth parameters. *Geochimica et Cosmochimica Acta*, *58*(1), 197–208. https://doi.org/10.1016/0016-7037(94)90457-X

De Villiers, S., Nelson, B. K., & Chivas, A. R. (1995). Biological Controls on Coral Sr/Ca and δ18O Reconstructions of Sea Surface Temperatures. *Science*, *269*(5228), 1247–1249. https://doi.org/10.1126/SCIENCE.269.5228.1247

Watanabe, T., Suzuki, A., Minobe, S., Kawashima, T., Kameo, K., Minoshima, K., et al. (2011). Permanent El Niño during the Pliocene warm period not supported by coral evidence. *Nature 2011 471:7337*, *471*(7337), 209–211. https://doi.org/10.1038/nature09777

Weber, J. N., & Woodhead, P. M. J. (1972). Temperature dependence of oxygen-18 concentration in reef coral carbonates. *Journal of Geophysical Research*, *77*(3), 463–473. https://doi.org/10.1029/JC077I003P00463

Westphal. (2015). A Quasi-Continuous Reconstruction of Central Tropical Pacific Climate Variability throughout the Mid-to Late Holocene Inferred from Line Island Fossil Corals. *ETH Zurich Library*. https://doi.org/10.3929/ethz-a-010659131

Wilks, D. S. (2019). *Statistical Methods in Atmoshperic Sciences*. (L. Kelleher & K. Zaliva, Eds.), *Statistical Methods in the Atmospheric Sciences*. Elsevier Inc. Retrieved from http://www.sciencedirect.com:5070/book/9780128158234/statistical-methods-in-the-atmospheric-sciences

Wold, S., Sjöström, M., & Eriksson, L. (2001). PLS-regression: A basic tool of chemometrics. *Chemometrics and Intelligent Laboratory Systems*, *58*(2), 109–130. https://doi.org/10.1016/S0169-7439(01)00155-1

Xing, W., Wang, B., & Yim, S. Y. (2016). Long-Lead Seasonal Prediction of China Summer Rainfall Using an EOF–PLS Regression-Based Methodology. *Journal of Climate*, *29*(5), 1783–1796. https://doi.org/10.1175/JCLI-D-15-0016.1